

Supplementary information

9,9'-spirobifluorene based zinc coordination polymers: a play on linker geometry and topology

Florian Moreau^{a,#}, Nathalie Audebrand^{a*}, Cyril Poriel^{a*}

^a Univ Rennes, ENSCR, INSA, CNRS, ISCR (Institut des Sciences Chimiques de Rennes) - UMR 6226, F-35000 Rennes, France

[#] *Now at* Institut des Matériaux Poreux de Paris, FRE 2000 CNRS, Ecole Normale Supérieure, Ecole Supérieure de Physique et de Chimie Industrielles de Paris, Paris Research University, 75005 Paris, France

Crystal structure of $Zn_2(L1)(H_2O)_2 \cdot (solv)_x$ (Zn-SBF-1)

Table S1. Selection of interatomic distances (Å) and bond angles (°) in $Zn_2(L1)(H_2O)_2 \cdot (solv)_x$ (Zn-SBF-1).

Within the paddle-wheel		Within the carboxylate functions	
Zn1- O17	1.998 (3)	C1-O4 ⁱⁱ	1.232 (4)
Zn1- O4	2.021 (2)	C1-O6	1.232 (4)
Zn1- O6	2.021 (2)	O4 ⁱⁱ -C1-O6	125.1 (3)
Zn1- O25	2.021 (3)	C27- O25	1.266 (5)
Zn1- O27	2.026 (3)	C27-O27 ⁱⁱ	1.222 (6)
Zn1-Zn1 ⁱ	2.967 (1)	O25-C27-O27 ⁱⁱ	125.00(4)

Hydrogen bond				
$D-H \cdots A$	$D-H$ (Å)	$H \cdots A$ (Å)	$D \cdots A$ (Å)	$D-H \cdots A$ (°)
C7—H7 ⁱⁱⁱ ⋯O4 ⁱⁱⁱ	1.100	2.410	3.481(5)	163.00

Symmetry codes: (i) $-x, -y, -z$; (ii) $1-x, -2-y, -z$; (iii) $x, -2-y, -3/2-z$

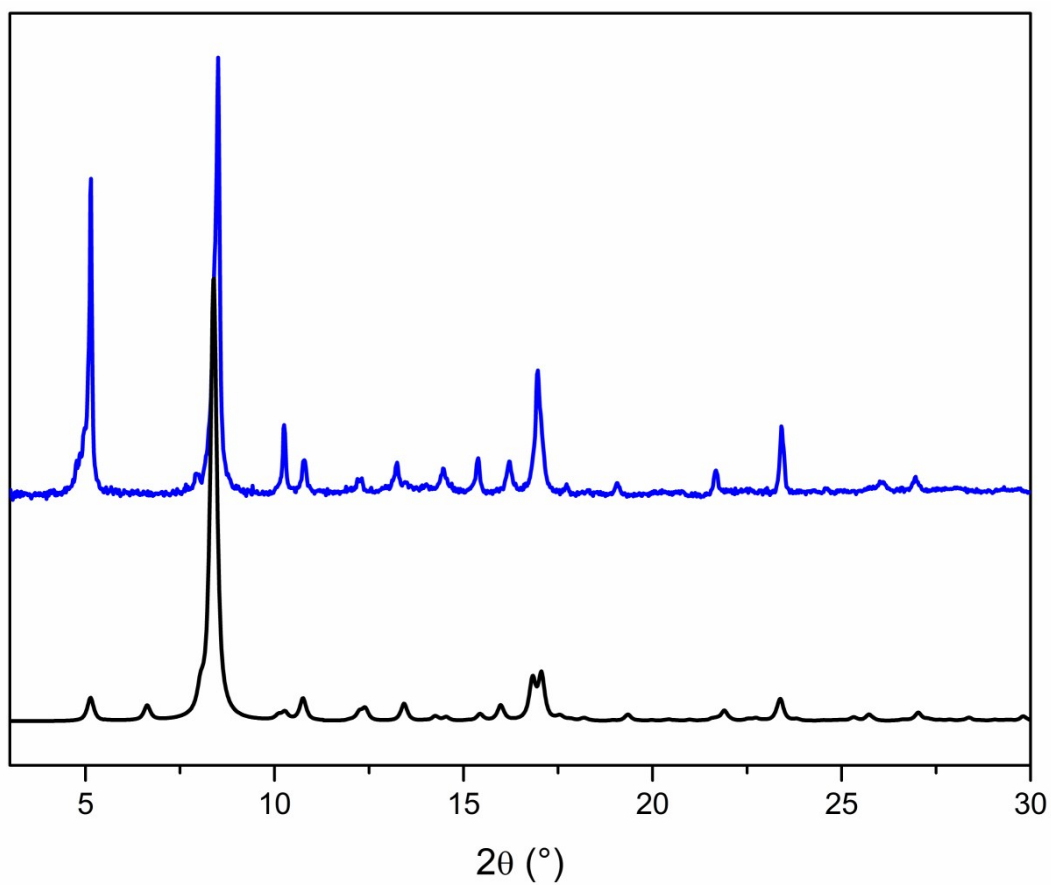


Figure S1. X-ray powder diffraction patterns of $\text{Zn}_2(\text{L1})(\text{H}_2\text{O})_2 \cdot (\text{solvent})_x$ (Zn-SBF-1); black: simulated from the crystal structure determined from single-crystal XRD data, blue: experimental.

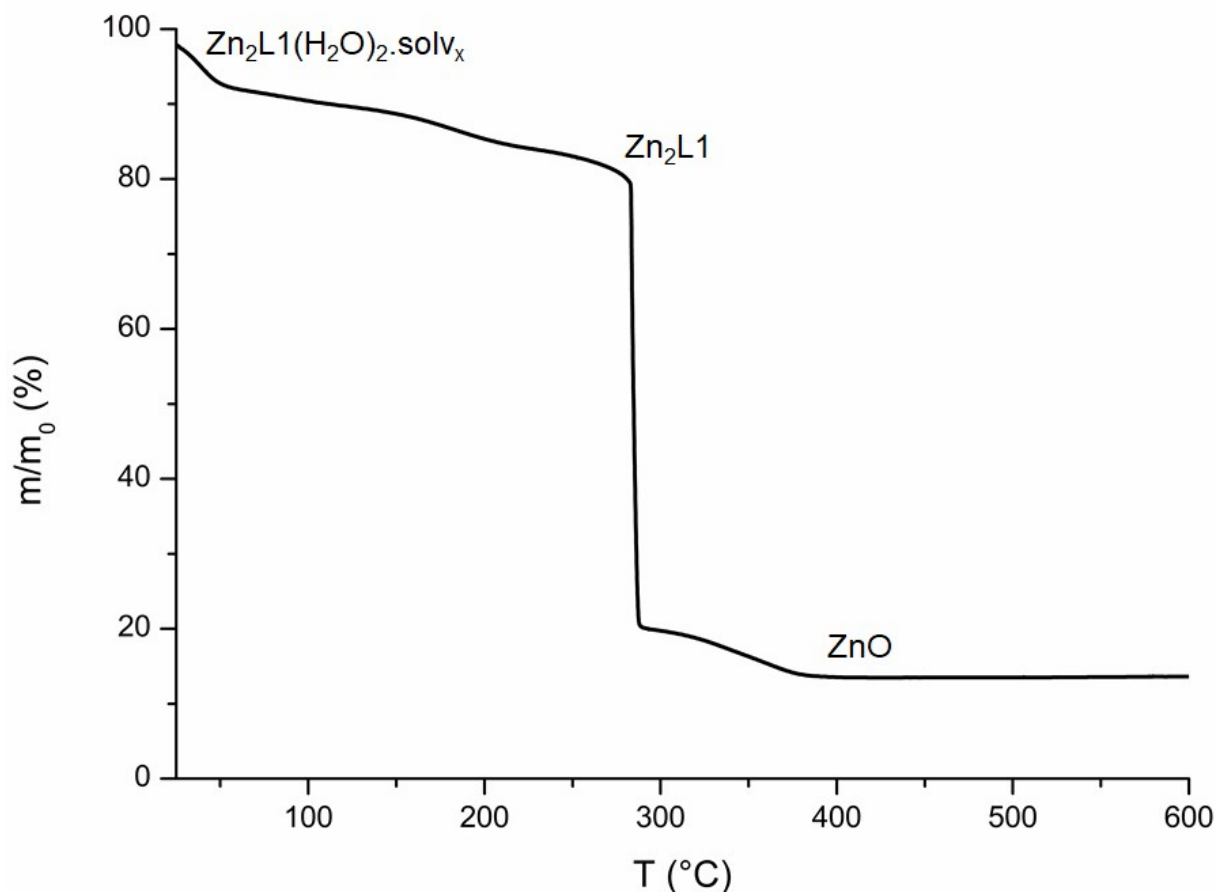


Figure S2. TGA under static air of $Zn_2(L1)(H_2O)_2 \cdot (solv)_x$ (*Zn-SBF-1*)

Thermogravimetric analysis (TGA) of **Zn-SBF-1** was performed on a Shimadzu TGA50 instrument in static air with a heating rate of $1.0 \text{ }^\circ\text{C}\cdot\text{min}^{-1}$ until $600 \text{ }^\circ\text{C}$ (Fig. S3). The powdered sample (c.a. 10 mg) was spread in alumina crucible.

Under heating treatment in static air, **Zn-SBF-1** exhibits a mass loss of 20 % between ambient temperature and $280 \text{ }^\circ\text{C}$ (Fig. S3). This loss corresponds to the departure of the solvent from the pores of the structure as well as coordinated water molecules, but it is rather difficult to elucidate the nature of this solvent molecules. For temperatures above $280 \text{ }^\circ\text{C}$, the decomposition of the framework occurs in two steps, and affords the final product ZnO ($m/m_0 = 13.54 \%$, $M = 488.45 \text{ g}\cdot\text{mol}^{-1}$).

Crystal structure of $Zn_2(L3)(DEF)_2(solv)_x$ (Zn-SBF-2)

Table S2. Selection of interatomic distances (Å) and bond angles (°) in $Zn_2(L3)(DEF)_2(solv)_x$ (Zn-SBF-2)

Within the inorganic SBU		Within the carboxylate functions	
Zn1-O1	1.947 (4)	Zn1-O4	2.033 (4)
Zn1-O3 ⁱ	1.950 (4)	C4-O2	1.258 (7)
Zn1-O2 ⁱⁱ	2.350 (4)	C4-O5	1.281 (6)
Zn1-O5 ⁱⁱ	2.071 (4)	O2-C4-O5	120.30(5)
		C15-O3	1.253(7)
		C15-O1	1.255(6)
		O1-C15-O3	126.20(5)

Hydrogen bonds				
$D-H \cdots A$	$D-H$ (Å)	$H \cdots A$ (Å)	$D \cdots A$ (Å)	
C11—H11 \cdots O5 ⁱⁱⁱ	1.100	2.410	3.419(8)	151.00
C19—H19 \cdots O5 ⁱⁱⁱ	1.100	2.240	3.276(8)	155.00
C1—H2 \cdots O1	1.100	2.530	2.94(2)	101.00
C1—H2 \cdots O2 ^{iv}	1.100	2.530	3.60(2)	163.00
C4—H4C \cdots O4	1.100	2.580	3.13(3)	109.00

Symmetry codes: (i) $-x+1/2, -y+1/2, -z$; (ii) $-x, y, -z+1/2$; (iii) $1/2-x, -1/2+y, 3/2-z$; (iv) $-1/2+x, 1/2-y, -1/2+z$.

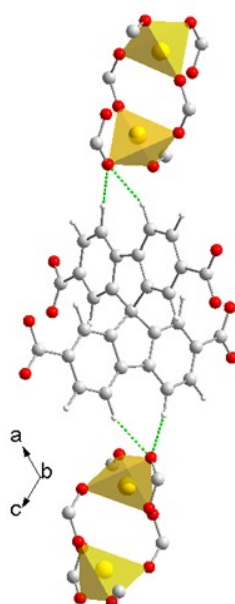


Figure S3. View of hydrogen bonds in $Zn_2(L3)(DEF)_2(solv)_x$ (Zn-SBF-2).

Crystal structure of $Zn_2(L3)(H_2O)_2 \cdot (solv)_x$ (Zn-SBF-3)

Table S3. Selection of interatomic distances (\AA) and bond angles ($^\circ$) in $Zn_2(L3)(H_2O)_2 \cdot (solv)_x$ (Zn-SBF-3)

Within the inorganic SBU		Within the carboxylate functions	
Zn1-O12	1.939 (4)	C18-O3	1.255 (6)
Zn1-O9	1.940 (4)	C18-O5	1.284 (6)
Zn1-O40	1.959 (4)	O3-C18-O5	124.10(5)
Zn1-O17	1.967 (4)	C38-O6	1.255 (7)
Zn2-O3	1.944 (4)	C38-O7	1.307 (7)
Zn2-O5 ⁱ	1.941 (4)	O6-C38-O7	119.10 (6)
Zn2-O7	1.999 (4)	C44 ⁱⁱ -O12	1.258 (6)
Zn2-O11	2.035(4)	C44-O40	1.275 (6)
		O12 ⁱⁱ -C44-O40	124.70 (5)
		C47-O9	1.276 (6)
		C47-O27	1.259 (7)
		O9-C47-O27	121.00 (6)

Symmetry codes: (i) 1-x, -y, 1-z; (ii) -x, 1-y, 2-z.

Crystal structure of $\text{Zn}_6(\text{L2})_3(\text{H}_2\text{O})_4 \cdot (\text{solv})_x$ (**Zn-SBF-4**)

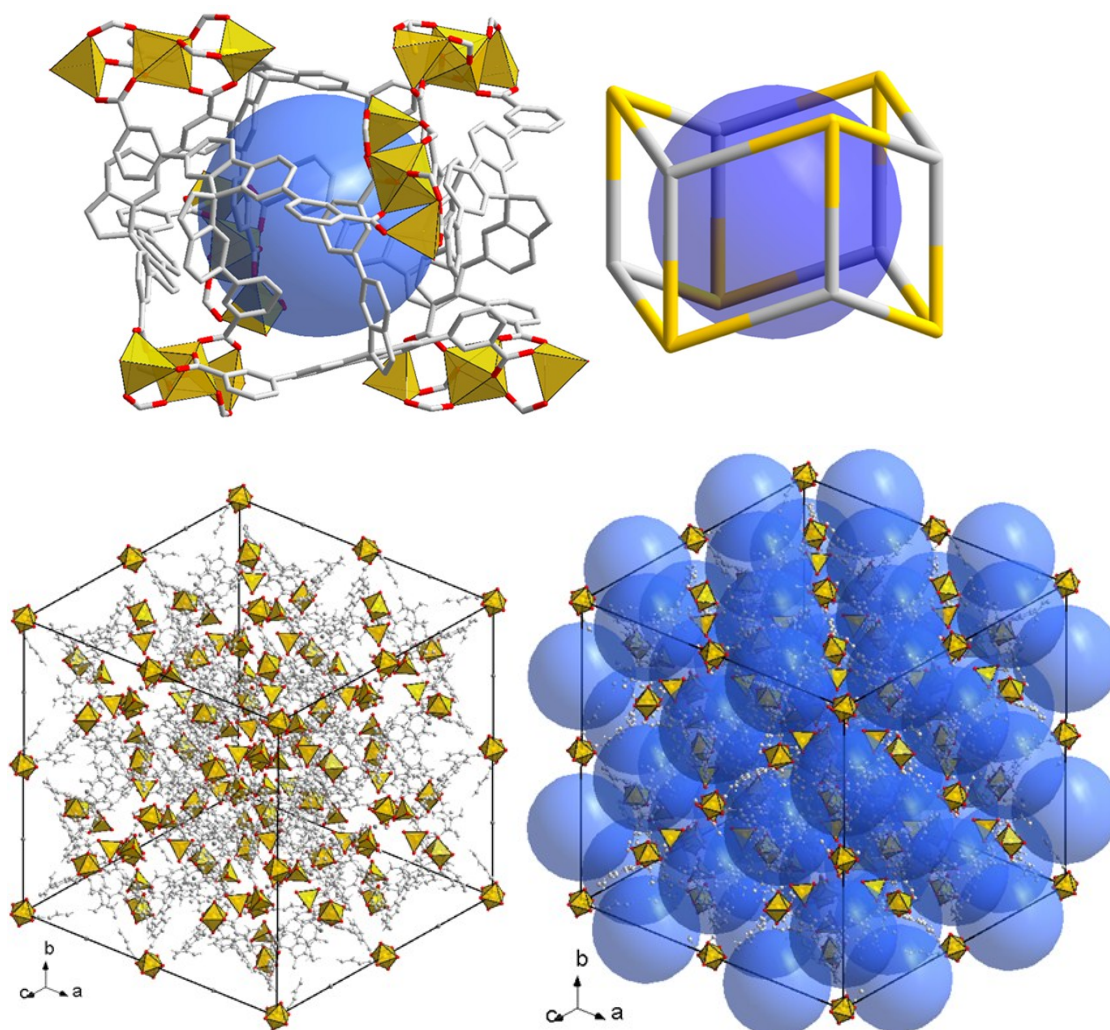


Figure S4. Views of the structure of $\text{Zn}_6(\text{L2})_3(\text{H}_2\text{O})_4 \cdot (\text{solv})_x$ showing the pores (blue spheres) and the *toc* topology.

The X-ray powder diffraction data of grounded crystals of **Zn-SBF-4** were collected at room temperature with a Siemens D500 diffractometer with the parafocusing Bragg-Brentano geometry, using monochromatic $\text{Cu K}\alpha_1$ radiation ($\lambda = 1.5406 \text{ \AA}$) selected with an incident beam curved-crystal germanium monochromator. The comparison between experimental X-ray powder diffraction pattern of ground crystals recorded at room temperature and theoretical pattern generated from the crystal structure determined at low temperature (Fig S3) shows that **Zn-SBF-4** undergoes a structural change during drying and grinding. Indeed, all the

diffraction lines are indexed in a monoclinic cell, demonstrating that the compound contains one unique phase, whose refined parameters are: $a = 22.595 (8) \text{ \AA}$, $b = 15.666 (3) \text{ \AA}$, $c = 22.177 (5) \text{ \AA}$, $\beta = 91.03 (2)^\circ$, $V = 7849 \text{ \AA}^3$ [$M_{20} = 9$, $F_{30} = 13 (0.0072; 319)$]. There is an important decrease of the symmetry comparing to the single-crystal structure although there are relationships between the lattice parameters of cubic single-crystal structure and

monoclinic cell determined from powder data ($a_m \approx c_m \approx \frac{1}{2} a_c$; $b_m \approx \frac{1}{2\sqrt{2}} a_c$).

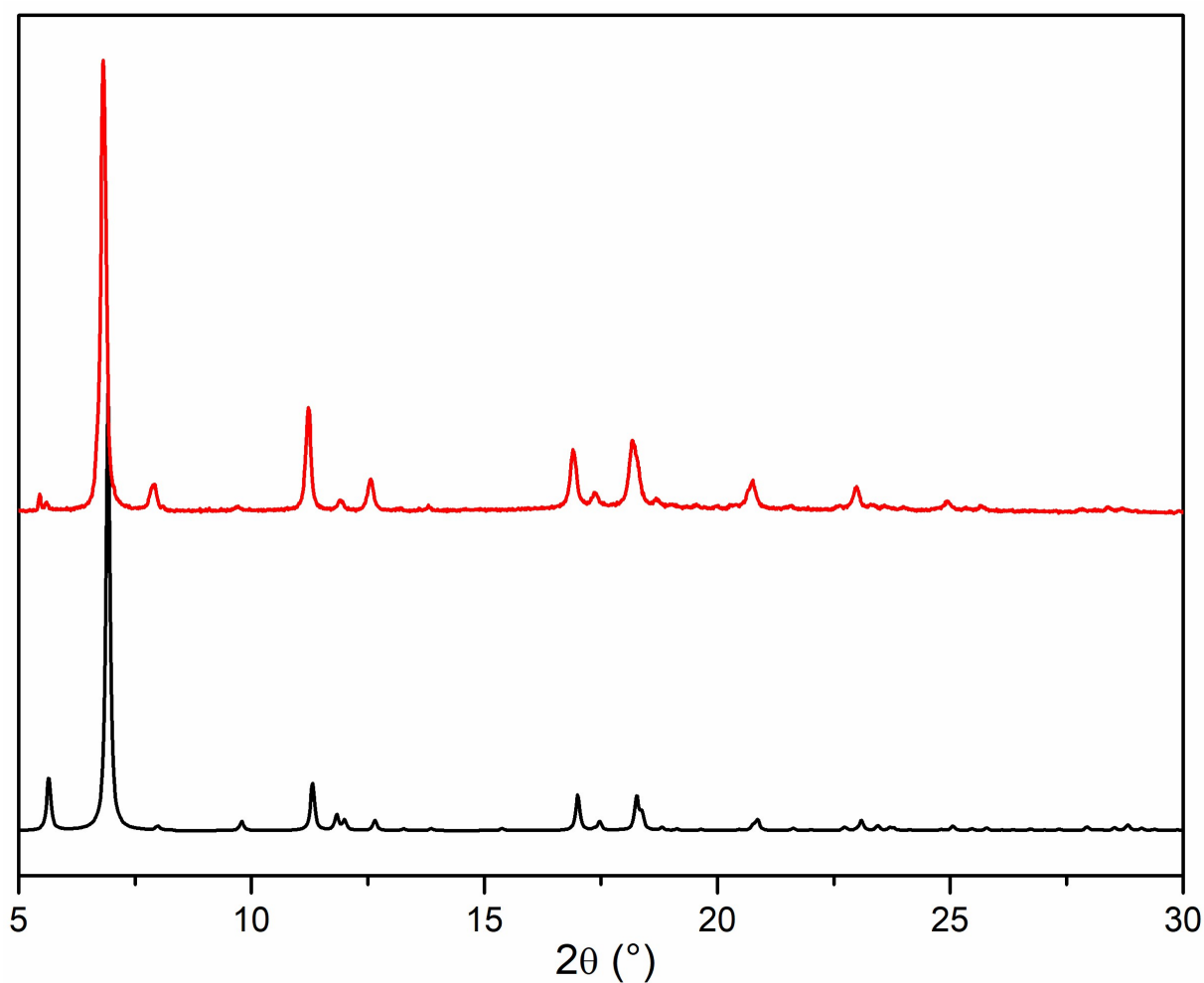
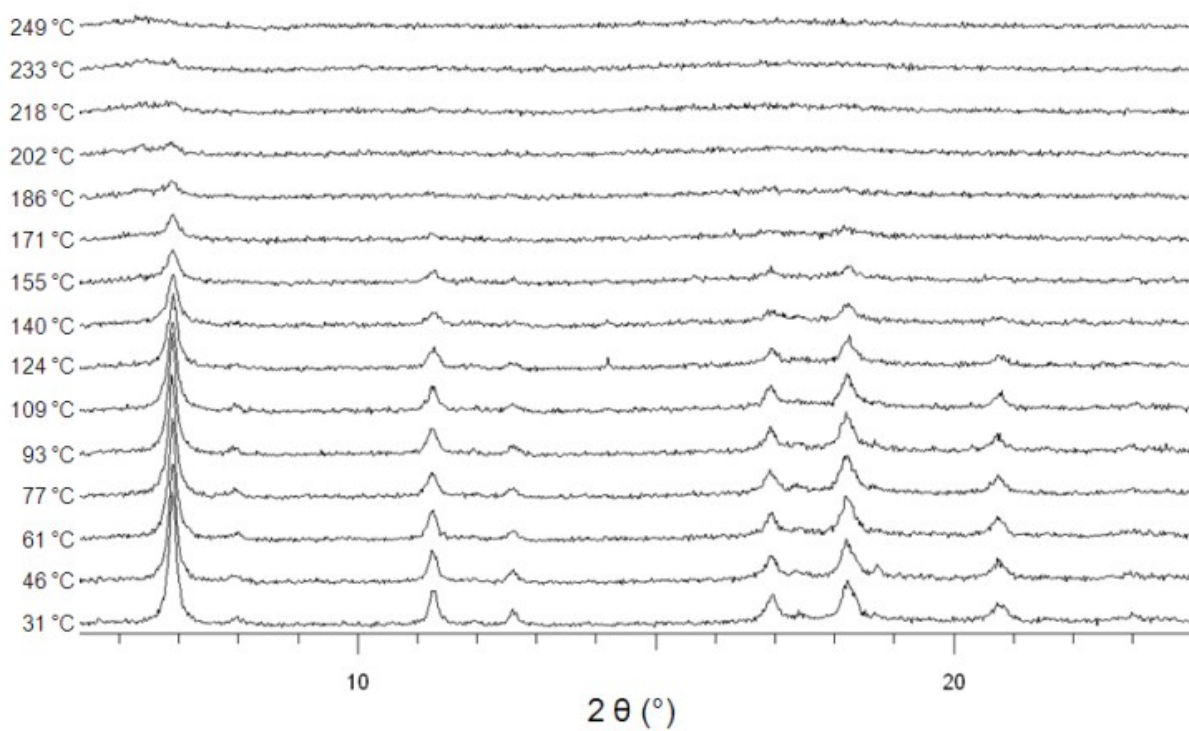
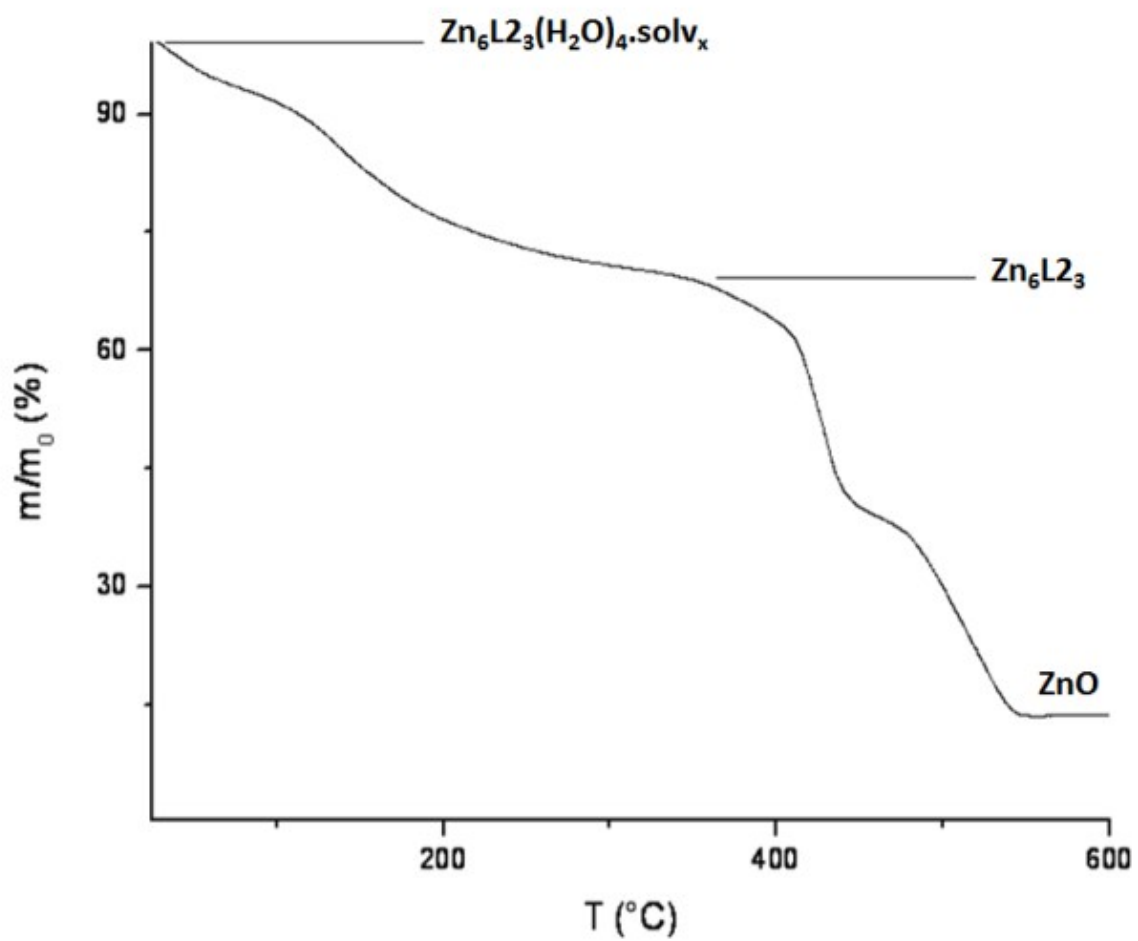


Figure S5. X-ray powder diffraction patterns of $\text{Zn}_6(\text{L}2)_3(\text{H}_2\text{O})_4(\text{sol}v)_x$; black: simulated from the crystal structure determined from single-crystal XRD data, red: experimental.

*Reactivity and thermal behavior and activation of **Zn-SBF-4***

Temperature-dependent powder X-ray diffraction (TDXD) of **Zn-SBF-4** was performed with a Bruker AXS D5005 diffractometer using a diffracted-beam-graphite monochromator ($\text{CuK}\alpha_{1,2}$) and equipped with a Anton Paar HTK1200 oven camera. Powder patterns were scanned over the angular range $5.00 - 25.00^\circ$ (2θ), step size 0.02° (2θ), step time 5 s step^{-1} . Sample has been heated in air between room temperature and 250°C with a heating rate of $1^\circ\text{C}\cdot\text{min}^{-1}$ between each powder pattern collected at constant temperature. Temperature calibration is carried out with standard materials in the given temperature range (Fig. **S4**).

Thermogravimetric analysis (TGA) of **Zn-SBF-4** was performed on a Shimadzu TGA50 instrument in static air with a heating rate of $1.0^\circ\text{C}\cdot\text{min}^{-1}$ until 900°C (Fig. **S4**). The powdered sample (c.a. 10 mg) was spread in alumina crucible.



a

b

Figure S6. TGA and TDXD under static air of $Zn_6(L_2)_3(H_2O)_4 \cdot (solv)_x$ (Zn-SBF-4).

Under heating treatment in static air, **Zn-SBF-4** exhibits a mass loss of 31 % between ambient temperature and 350 °C (Fig. **S4**). This loss corresponds to the departure of the solvent from the pores of the structure, but it is rather difficult to elucidate the nature of this solvent molecules. At 350°C, the compound exhibits a m/m_0 of 69 %, which is consistent with the formula of the desolvated compound $Zn_6L_2_3$ (M_{theor} : 2770.8 $\text{g}\cdot\text{mol}^{-1}$; M_{exp} : 2490 $\text{g}\cdot\text{mol}^{-1}$). Finally, for temperatures above 400 °C, the decomposition of the framework occurs in two steps, and affords the final product ZnO ($m/m_0 = 13.54$ %, $M = 488.45$ $\text{g}\cdot\text{mol}^{-1}$).

In situ X-ray powder diffraction as a function of temperature showed that the crystallinity of the MOF decreases from 100° C leading at 170° C to an amorphous product (Fig. **S4**). This loss of crystallinity corresponds to the first step of mass loss and occurs at a relatively low temperature. Then, it seems impossible to eliminate most of the solvent from the pores by simple heating without destroying the crystal structure. MOF activation by conventional heating at moderate temperatures (below 100 ° C) under vacuum resulted also in amorphous compounds. The ligand flexibility allowed by the rotation of benzoate groups around the C6-C8 axis joining the SBF core to benzoate (see Fig. 10 in main text) can allow the network to collapse when crystallization solvent molecules starts to evacuate. It is also probable that the activation process led to the departure of coordinated water molecules from inorganic SBU, which alter the coordination sphere of zinc atoms initially in tetrahedral environment, and then also would lead to the collapse of the structure.

Table S4. Selection of interatomic distances (Å) and bond angles (°) in $Zn_6(L_2)_3(H_2O)_4(\text{solv})_x$

Within the carboxylate functions			
C14-O3	1.276 (4)	C14-O4	1.247 (4)
O3-C4-O4	124.00 (3)		
Within the inorganic SBU			
Zn1—O4 ⁱ	2,084 (2)	Zn1—O4	2,084 (2)
Zn1—O4 ⁱⁱ	2,084 (2)	Zn2—O3 ⁱⁱ	1,933 (2)
Zn1—O4 ⁱⁱⁱ	2,084 (2)	Zn2—O3	1,933 (2)
Zn1—O4 ^{iv}	2,084 (2)	Zn2—O3 ^{iv}	1,933 (2)
Zn1—O4 ^v	2,084 (2)	Zn2—O5	1,992 (5)

Symmetry codes: (i) $-z+1, x-3/4, y+1/4$; (ii) $-y+3/4, -z+1/4, x-1/2$; (iii) $y+3/4, z-1/4, -x+1$; (iv) $z+1/2, -x+3/4, -y+1/4$; (v) $-x+3/2, -y, -z+1/2$.